Canadian Mineralogist
Vol. 24, pp. 479-497 (1986)

STRUCTURAL MODULATIONS IN IRON-RICH AND MAGNESIUM-RICH MINNESOTAITE

STEPHEN GUGGENHEIM

Department of Geological Sciences, University of Illinois at Chicago, Chicago, Illinois 60680, U.S.A.

RICHARD A. EGGLETON

Department of Geology, Australian National University, Canberra, A C T 2600, Australia

ABSTRACT

Magnesian minnesotaite has a dominant primitive lattice with a = 28.0 Å ($\sim 5 \times a_{\text{talc}}$), b = 9.4 Å, d_{001} = 9.6 Å, c = 12.4 Å, α = 101°, β = 127°, γ = 90°, Z = 1, with an ideal composition of $(\text{Fe,Mg})_{30}\text{Si}_{40}\text{O}_{96}(\text{OH})_{28}$. Ferroan minnesotaite is dominantly C-centred with a = 50.6 Å ($\sim 9 \times a_{\text{talc}}$), b = 9.6 Å, d_{001} = 9.6 Å, c = 12.4 Å, α = 101°, β = 127°, γ = 90°, Z = 2 and an ideal composition of $(\text{Fe,Mg})_{27}\text{Si}_{36}\text{O}_{86}(\text{OH})_{26}$. The Mg:Fe ratio is about 0.2 for the C-centred structure and ranges between 0.2 and 0.75 for the primitive structure. Twinning and complex intergrowths between P and C cells produce reflections simulating a superlattice along Y and Z. Each of the two types shows a discrete variation in β^* angle, commonly measured as 42°, 52° and 64°. Diffuse streaking is observed along reciprocal lattice rows parallel to Z^* for $k \neq 6n$ on nets of $0kl$ reflections, with lesser amounts of streaking parallel to X^* and Z^* on $h0l$ nets. A structural model for minnesotaite is derived from $k = 3n$ subcell X-ray data, electron-optical structural images, and simulation of electron-diffraction data by optical diffraction. A 2:1 layer is approximated by a continuous octahedral sheet and opposing tetrahedral sheets, with the latter modulated along X, but continuous along Y. The P cell has tetrahedral strips that are four tetrahedra wide, whereas the C cell has three-tetrahedra-wide strips regularly alternating with four-tetrahedra-wide strips. For both structures, adjacent strips are connected by a single chain of silicon–oxygen tetrahedral chain extending parallel to Y and occupying the interlayer region. Thus, adjacent strips within the sheets and across the interlayer region are firmly linked. Across the octahedral sheet opposing tetrahedral strips are displaced parallel to X by one half of a strip width, allowing a corrugation to develop in the layers with limited curving of the tetrahedral–octahedral interface. It is postulated that the origin of the supercell is based on dimensional misfit between a continuous Si tetrahedral sheet and an ideally flat iron-rich octahedral sheet. Consequently, ten tetrahedra (4+1+4+1) span nine octahedra parallel to X for the P cell. For the C cell with the larger, iron-enriched octahedra, nine tetrahedra (4+1+3+1) span eight octahedra.

Keywords: minnesotaite, talc (iron), modulated structure, X-ray, high-resolution transmission electron-microscopy.

SOMMAIRE

La minnesotaïte magnésienne a un réseau primitif: $a = 28.0\,(\sim 5a_{\text{talc}})$, $b = 9.4$, $d_{001} = 9.6$, $c = 12.4$ Å, α = 101°, β = 127°, γ = 90°, Z = 1, avec formule $(\text{Fe,Mg})_{30}\text{Si}_{40}\text{O}_{96}(\text{OH})_{28}$. La minnesotaïte ferreuse possède une maille à face C centrée: a = 50.6 ($\sim 9\ a_{\text{talc}}$), b = 9.6, d_{001} = 9.6, c = 12.4 Å, α = 101°, β = 127°, γ = 90°, Z = 2, et répond à la formule $(\text{Fe,Mg})_{27}\text{Si}_{36}\text{O}_{86}(\text{OH})_{26}$. Le rapport atomique Mg/Fe est d'environ 0.2 pour la structure à réseau C, mais varie de 0.2 à 0.75 pour la structure à réseau P. Le maclage et des intercroissances complexes entre structures P et C produisent des réflexions qui simulent un surréseau en Y et Z. Chacun des deux types structuraux montre une variation de l'angle β^*, dont les valeurs mesurées sont le plus souvent 42°, 52° et 64°. On observe, sur réticules des réflexions $0kl$, le long des rangées du réseau réciproque parallèles à Z^*, des traînées diffuses pour $k \neq 6n$; sur les réticules des réflexions $h0l$, des traînées analogues, mais moins marquées, suivent les directions X^* et Z^*. On peut construire un modèle structurel de la minnesotaïte à partir des données roengenographiques pour la maille sous-multiple $k = 3n$, des images structurelles dans l'optique à électrons, et la simulation des données de diffraction électronique par diffraction optique. En première approximation, une couche 2:1 peut se concevoir comme continue: couche d'octaèdres flanquée de couches tétraédriques opposées, discontinues le long de X, mais continue le long de Y. Dans la structure P, les bandes tétraédriques sont larges de quatre tétraèdres; dans la structure C, deux types de bandes alternantes sont larges, respectivement, de trois et de quatre tétraèdres. Dans les deux types de structure, deux bandes contigües sont reliées par une chaîne de tétraèdres à silicium, parallèle à Y, située dans l'intercouche. Les bandes d'une même couche sont donc fortement unies. les bandes tétraédriques opposées, de part et d'autre de la couche octaédrique, sont déplacées l'une par rapport à l'autre, parallèlement à X d'une demi-largeur de bande. Il en résulte une corrugation des couches, avec une certaine courbure de la surface de contact entre tétraèdres et octaèdres. Notre conjecture quant à l'origine du surréseau s'appuie sur la différence de dimensions entre la couche tétraédrique continue et la couche octaédrique, riche en fer, idéalement plane. En conséquence, dix tétraèdres (4 + 1 + 4 + 1) embrassent neuf octaèdres parallèlement à X, dans la structure P, tandis que, dans la structure C, où les octaèdres à fer sont plus grands, neuf tétraèdres (4 + 1 + 3 + 1) embrassent huit octaèdres.

Mots-clés: minnesotaïte, talc (avec Fe), structure modulée, rayons X, TEM, HRTEM.

INTRODUCTION

The common layer-silicate minerals have structures in which sheets of corner-linked tetrahedra are co-ordinated to sheets of edge-connected octahedra. These sheets may be connected in a ratio of either 1:1 (*i.e.,* serpentine) or 2:1 (*i.e.,* talc, pyrophyllite, micas) to form a larger unit known as a layer. Adjacent layers may be linked by long hydrogen bonds, as in the serpentines, or by van de Waals bonds, as in talc or pyrophyllite. Alternatively, linkages may be formed by various interlayer materials such as cations, hydrated cations, and metal–hydroxyl octahedral sheets, in the micas, smectites, and chlorite minerals, respectively. The diversity of interlayer connections acceptable between 2:1 layers suggests that the layers themselves impose minimal restrictions on the nature of the interlayer bonding.

In contrast to the junction at the interlayer region, the linkage between the component tetrahedral and octahedral sheets is quite restricted because the apical oxygen atoms of the tetrahedral sheet are shared with the co-ordination polyhedra of the octahedral sheet. This common plane of junction requires that the tetrahedral and octahedral sheets have equal or nearly equal lateral dimensions. However, variations in the unconstrained lateral dimensions of these two component sheets are common, and two general mechanisms have been observed that compensate for the misfit: either a chemical substitution in either or both component sheets, or a structural adjustment. For example, there is either little or no difference in lateral dimension of the two component sheets in the serpentine lizardite, because Al^{3+} substitutes for both Si^{4+} and Mg^{2+}, thereby enlarging the lateral dimensions of the silicate tetrahedral sheet and reducing the size of the octahedral sheet, while still maintaining charge balance. If chemistry does not ameliorate all misfit in lizardite, presumably congruence is achieved by small distortions in the tetrahedral and octahedral polyhedra.

Structural adjustments vary considerably depending on the amount of strain at the junction and the flexibility of the component sheets. Where the ideal lateral dimensions of a tetrahedral sheet are larger than those of an octahedral sheet, as is common in the micas, Zviagin (1957) and Radoslovich (1961) have shown that the tetrahedral sheet can easily reduce its size by in-plane rotations of adjacent tetrahedra in opposite directions. Enlargement of a sheet of tetrahedra by structural adjustment to allow congruence with the octahedral sheet is more difficult, and often both sheets must deform or be modulated. In 1:1 layer silicates, observed modifications include: (1) out-of-plane tilting of tetrahedra to form the cylinder-like coiled structure of chrysotile (Jagodzinski & Kunze 1954), (2) tetrahedral tilting with periodic inversions at four- and eight-fold rings to form the wave-like structure of antigorite (Zussman 1954, Kunze 1956) and (3) tilting of tetrahedra with periodic inversions of three- and four-fold rings to produce the domed island-like structures of greenalite and caryopilite (Guggenheim *et al.* 1982). Modifications involve vacancies in the sheet of octahedra at the inversion point in the tetrahedral sheet, as has been suggested for antigorite, greenalite and caryopilite. Bailey (1980) provided a recent summary.

Excessive out-of-plane tilting of tetrahedra cannot occur in the 2:1 layer silicates because identical sheets on opposite sides of a common octahedral sheet hold it flat under tension. To provide for a better fit between sheets of tetrahedra and octahedra in 2:1 layer silicates, structural accommodations have been found to include: (1) the adjustment of sheet thicknesses with a corresponding change in lateral dimensions, as in sudoite (Eggleton & Bailey 1967), (2) a reversal and relinkage of apices of tetrahedra, as in stilpnomelane (Eggleton 1972) or ganophyllite (Eggleton & Guggenheim 1986), and (3) a modified geometry of sheets to include three-fold rings as in zussmanite (Lopes-Vieira & Zussman 1969) or five- and seven-fold rings, as in bannisterite (I.M. Threadgold, pers. comm., 1979). Limited tilting of tetrahedra may occur along with the other structural accommodations, as has been found in stilpnomelane, bannisterite and ganophyllite.

Minnesotaite is an iron-rich hydrous layer-silicate that commonly occurs in silicate iron-formations metamorphosed to a low grade (Leith 1903, Gruner 1944). Gruner suggested that minnesotaite is the ferrous iron analogue of talc, based on X-ray powder photographs of impure material. However, an octahedral sheet rich in ferrous iron is too large to link laterally with a Si-rich tetrahedral sheet without a structural reorganization. Although the *d*(001) value of approximately 9.6 Å suggests a 2:1 layer silicate like talc, Guggenheim & Bailey (1982) found that the structure is modulated by a superlattice along each of its three axes. The superlattice along X^* is well defined for the twin that was studied and shows a repeat of at least nine times the normal *a*-axis repeat on the *h*0*l* and *hk*0 nets. However, other subcell zones indicated a further doubling of *a*, leading to a superlattice *a* axis eighteen times that of the subcell a_0. Likewise, the *b*-axis repeat was found to extend to $6b_0$ and the *c* axis was tentatively assigned a superlattice of twelve c_0. Twinning does not cause superposition of subcell reflections; the X-ray powder data were indexed and subcell dimensions refined by Guggenheim & Bailey (1982).

Both the chemistry (see below) and the X-ray data suggest that the minnesotaite structure is similar to the 2:1 talc structure, but with either one or both types of sheets modulated. The purpose of this study is to determine the nature of the structural accommodation that takes place in minnesotaite.

COMPOSITION OF MINNESOTAITE

All analyzed samples (Table 1) have been shown

TABLE 1. CHEMICAL ANALYSES OF MINNESOTAITE AND PREDOMINANT TYPE OF CELL

	1a	1b	2	3a	3b	4a	4b	5	6-1	6-2	6-3	6-4	6-5	7
SiO_2	51.79	49.75	49.41	50.14	49.77	51.47	51.00	51.04	51.50	52.14	51.89	52.37	53.39	53.85
Al_2O_3	1.46	1.85	0.68	0.37	0.33	1.57	1.76	0.09	0.47	0.39	0.38	0.36	0.21	0.15
Fe_2O_3	0.61	38.31	16.34	2.00	39.23	3.23	33.49	35.64	33.60	32.13	33.54	31.20	26.78	30.53
FeO	35.65		24.19	36.68		30.50								
MnO	0.78	0.85	0.65	0.27	0.14	1.83	3.41	0.47	b.d.	0.12	b.d.	b.d.	b.d.	0.53
MgO	3.21	3.34	2.95	4.39	4.08	5.10	5.03	5.39	7.32	7.33	7.92	8.43	11.01	9.68
CaO	0.10	*b.d.	0.02	0.1		b.d.	0.05	0.01	b.d.	0.10		b.d.	b.d.	0.03
Na_2O	0.06	0.11	0.03	0.05			0.25	0.17		b.d.			b.d.	0.15
K_2O	0.44	0.54	0.07	0.15	0.12		0.024	0.17	0.31	0.39	0.21	0.53	0.38	0.17
H_2O^+	5.03		5.20	5.24		5.88								
H_2O^-	0.03		0.38	0.44		0.16								
CO_2	0.14		0.22											
S			0.05											
C			0.15											
P_2O_5	0.08		0.08	0.01										
TiO_2	0.08		b.d.	0.02										
F	0.02													
TOTAL	99.43	94.75	100.42	99.86	93.78	99.74	95.13	92.99	93.20	92.62	93.95	93.05	91.78	95.09
LESS	0.01		0.02											
TOTAL	99.42		100.40											
BASED ON CATION CHARGE OF +22														
Si	4.00	3.88		3.91	3.93	3.93	3.90	3.99	3.96	4.00	3.95	3.98	4.02	3.98
Al	0.13	0.17		0.03	0.03	0.14	0.16	0.01	0.04	0.04	0.03	0.03	0.02	0.01
Fe^{3+}	0.04	2.50		0.12	2.59	0.19	2.14	2.33	2.16	2.06	2.14	1.98	1.69	1.89
Fe^{2+}	2.30			2.40		1.95								
Mn	0.05	0.06		0.02	0.01	0.12	0.22	0.03		0.01				0.03
Mg	0.37	0.39		0.51	0.48	0.58	0.57	0.63	0.84	0.84	0.90	0.96	1.24	1.07
Ca	0.01			0.01						0.01				0.01
Na	0.01	0.02		0.01			0.04	0.03						0.02
K	0.04	0.05		0.02	0.01		0.02	0.02	0.03	0.04	0.02	0.05	0.04	0.02
OH	2.60			2.96		3.08								
PREDOMINANT CELL TYPE														
	C		**d	P		d		P	P					P

* Below detection **Disordered along X*

1. Labelled as sample No. BM 131 from the Sagamore pit, Cuyuna district, Minnesota by Blake (1965). The analysis has been adjusted to remove elements resulting from stilpnomelane, opaques, carbonates and contaminating P_2O_5 and TiO_2, 1a wet analysis reported by Blake (1965); 1b probe analysis.
2. Labelled as sample No. 60GF 133 and collected by G. A. Gross one mile northwest of the French Mine on the slope northwest of Pete signal, near Schefferville, Quebec. G. A. Bender, analyst.
3. Labelled as sample No. GF M-1 coming from a drill hole in the Schefferville, Quebec area located in the Sokoman Iron Formation. 3a wet analysis by J. L. Bower; 3b probe analysis.
4. From the Blue Bell Mine, Riondel, British Columbia. 4a wet analysis from Perrault & Hébert (1968); 4b probe analysis.
5. From the Knob Lake area, Quebec (near Schefferville). Probe analysis.
6. From the Auburn Mine, Minnesota. Probe analysis.
7. Labelled as sample No. DC-21 from the Lean Chert member of the Sokoman Iron Formation approximately one mile southeast of Ardua Lake, Quebec, and given as probe analysis M-5 in Lesher (1978).

through TEM studies to contain impurities, commonly stilpnomelane, graphite, greenalite, quartz, magnetite and other (unidentified) phases. Therefore, differences in bulk chemistry may not be pertinent to the composition of minnesotaite. The most reliable analyses (Table 1, 1a and 7) are those of Blake (1965) and Lesher (1978). Blake made great efforts to determine the effects of each contaminant and could subtract out impurity components. Only quartz and magnetite are associated with the Sokoman sample (Anal. 7), and it is possible to avoid contaminated areas during analysis by electron microprobe. Small amounts of Ca, Na and K, especially in the Sokoman sample, suggest that the minnesotaite structure has a limited capacity to accommodate the alkali elements.

Results of four wet-chemical analyses (Tables 1, 1a, 2, 3a and 4a) are given along with electron-microprobe data for comparison. Although it is likely that the iron was partly oxidized during the analysis of sample 2, the results are of interest to establish hydroxyl content. Within the accuracy of the analyses, water content for the three samples appears consistent. Calculated formulae show a significant excess of hydroxyl in minnesotaite in comparison to that in talc.

Analyses of samples from the Auburn mine show a range of compositions consistent with substitution of iron for magnesium. However, such analyses cannot determine whether individual grains are of the reported composition or whether grains of distinctly different compositions average to the reported bulk-composition.

X-RAY STUDY

The subcell

Single-crystal X-ray data were obtained for the subcell reflections on material from the Cuyuna district of Minnesota. Precession photographs and (Gandolfi) powder data from the single crystal used in this study were presented by Guggenheim & Bailey (1982). The crystal was mounted on the c^* axis and data collected on a Picker FACS-1 single-crystal diffractometer using Mo$K\alpha$ radiation. The specimen shows extra reflections, about midway between subcell reflections, indicating that it is a twin. However, the contrast in mosaic spread between the two groups of subcell reflections, the differences in intensities of the two sets, and the close agreement between the relative intensities of the predominant set, as measured by the single-crystal diffractometer and from the Gandolfi film, suggest that the extra reflections (those of the second component crystal) do not superimpose with the subcell reflections of the first component crystal in the twin.

Because of large mosaic spread, reflections were collected in an omega-scan mode, with scan widths of 4.25°. Scan speed was 1°/min, and background counts were made for 20 seconds. Intensity measurements, collected for the entire reciprocal sphere to $2\theta = 40°$, yielded 2645 reflections, including twin reflections. Crystal and electronic stability were monitored by comparing a set of three standard reflections taken every 50 observations. The data were corrected for Lorentz and polarization effects. The $00l$ type reflections (l from 2 to 13) were collected by taking ψ scans (*i.e.*, rotating the crystal approximately about the diffraction vector) and measuring intensities at each 10° increment in ϕ. The resulting 36 measurements of intensity per $00l$ reflection were then used to correct empirically for absorption (North *et al.* 1968). Absorption was found to be considerable; variations in intensity within a grouping of the 36 reflections amount to as much as 60%.

Reflections were considered observed for $I > 3\sigma$, where the standard deviation σ of the intensity I is defined as $\sigma(I) = [c + 0.25(t_c/t_b)^2(B_1 + B_2) + (pI)^2]^{1/2}$, where c is the total integrated counts in time t_c, B_1 and B_2 are the background counts in time t_b, p is arbitrarily chosen as 0.03, and $I = [c - 0.5(t_c/t_b)(B_1 - B_2)]$. Reflections were collected by using a pseudohexagonal unit-cell and then transformed to the *C*-centred cell given by Guggenheim & Bailey (1982). This cell is analogous to that of talc. The data were averaged to four octants for evaluation in space group $C\bar{1}$. There are 496 unique reflections from the main component, 304 of which are considered to be of zero intensity. Of the 192 observed reflections, there are twelve $00l$ and 62 $h0l$ reflections. All observed reflections have $k = 3n$.

One-dimensional electron-density projection. In layer silicates, the $00l$ reflections are least likely to be affected by twinning. One-dimensional electron-density maps were calculated by determining the phases based on a talc structure (z co-ordinates), with iron scattering factors for the octahedral occupancy. That is, it was assumed that the minnesotaite structure is a modification of a 2:1 layer silicate, an assumption that was confirmed by high-resolution imaging (see below).

The resulting electron-density map shows significant electron-density in the 'interlayer' region at $z = 0.5$. The ratio of peak heights at $z = 0.11$ (apical oxygen + OH) to $z = 0$ (Fe ions) is 0.31. This ratio is in agreement with the expected value for a talc-like octahedral sheet, in which the heavy atom is co-ordinated by six oxygen atoms and OH groups.

Based on the electron-density maps, approximately 13 electrons per three iron atoms are required in the interlayer space. Several maps were calculated by removing scattering material at $z = 0.29$ (Si) and $z = 0.36$ (basal oxygen atoms) and adding electrons at $z = 0.5$. The residual R improved considerably: R_{00l} for no interlayer material, as in an Fe-talc structure, is 0.27, whereas R_{00l} for the model with interlayer material is 0.05. Figure 1 shows the resulting direct-Fourier and difference-Fourier maps.

The residual R is not sensitive to variations in scattering material taken from either Si or basal oxygen positions for placement at $z = 0.5$. Therefore, it is not possible from these data to determine the proportion of Si and basal oxygen atoms required to total 13 electrons in the interlayer region.

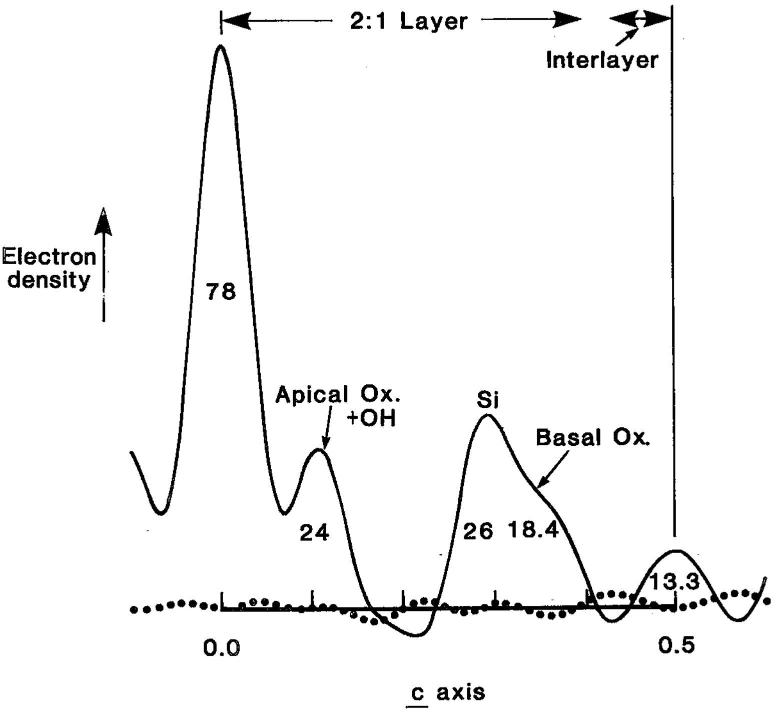

FIG. 1. One-dimensional electron-density map for minnesotaite from the Cuyuna district, Minnesota. Numbers under the curve represent integrated intensities, in electrons, of the corresponding resolved peaks. The largest peak represents the electron count of 78 electrons of octahedral iron, Fe_3. The dotted line is the resulting Fourier difference-map. The residual (R) value is 0.05.

Two-dimensional analysis. With the structure factors phased by the iron ions and co-ordinating oxygen atoms and OH groups, an $h0l$ direct-Fourier map was calculated. Additional peaks were located that are consistent with silicon and basal oxygen atoms in an arrangement similar to that in talc. However, electron-density peaks for the silicon atoms in talc-like silicon positions have densities equivalent to only 0.74 silicon atoms rather than 1 as in talc. Furthermore, the basal oxygen located directly below the silicon was not found as a discrete peak in the map. However, the silicon peak is sufficiently diffuse and strong that this basal oxygen, which is closest to the silicon in projection, may be unresolved.

Two additional peaks were located in the interlayer region (x,z; 0.45, 0.5; 0.1, 0.5), each about 7.5 electrons (equivalent in height to 2 × 0.26 silicon atoms) in height. The iron and silicon atoms show considerable elongation along Z^* and were included in successive Fourier calculations split into two half-atoms, slightly displaced along Z^*. Attempts to refine the structure were unsuccessful, indicating that the limits of the data for this model had been reached. The residual R for the model that includes 'half-atom' iron ions, all basal oxygen atoms, interlayer scattering material and two scale factors (one for $00l$ and another for all other $h0l$ reflections) is 0.121 (R_1) and 0.110 (R_2).

ELECTRON-OPTICAL STUDY

All the samples given in Table 1 were examined by electron microscopy on a JEOL 100CX, and samples from the Cuyuna district (Blake 1965) and the Sokoman Iron Formation (Lesher 1978) were examined also on a JEOL 200CX electron microscope. For diffraction patterns and optical-imaging techniques near the basal plane, samples were prepared by abrading minnesotaite-rich rock with an iron file and further dispersing the particles in alcohol with an ultrasonic vibrator. For examination, a drop of alcohol with the dispersed particles was placed on a holey carbon grid and allowed to evaporate. It is noteworthy that minnesotaite, like most layer silicates, shows perfect cleavage on the (001) plane. However, imperfect cleavage is also observed, on the (010) plane.

For diffraction patterns and optical-imaging studies at orientations far from the basal plane, sam-

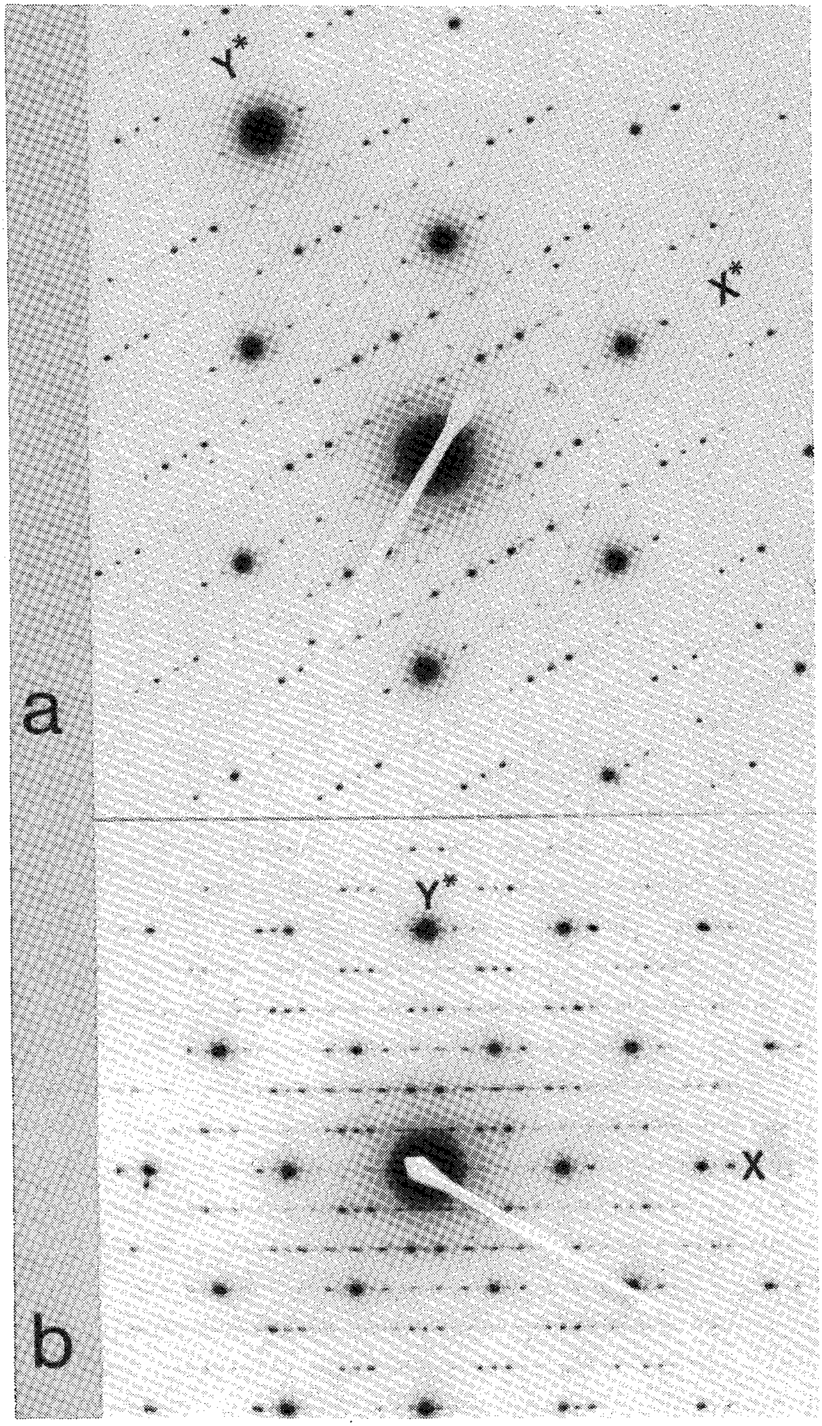

FIG. 2a. The *hk*0 net of the *P* cell of minnesotaite from Ardua Lake, Quebec. Of particular note are the strong subcell reflections on $k = 3n$ layer lines and the triplets of more intense superlattice reflections. (b) The basal plane net shows features similar to those of the *hk*0 net, except for subtle differences in intensity of subcell reflections. This net is related to Figure 2a by a 21° rotation about Y^*.

ples were prepared by conventional Ar ion-thinning techniques. Samples studied in the JEOL 100CX could be placed in a tilt–rotate or a double-tilt stage, both with ±60° tilt axes. In this way, all orientations of the reciprocal lattice could be examined, and it was possible to relate the different sets of principal planes of diffraction. The JEOL 200CX has sample-tilt restrictions of ±10°.

Minnesotaite consists of two structural modifications, one primitive ($P\bar{1}$), the other one face-centred ($C\bar{1}$); an apparently single crystal commonly exhibits both. In addition, twinning and one-dimensional disorder in several directions are common. Therefore, for simplicity, diffraction data are presented in two parts, based on the primitive cell modification and the C-centred cell variant.

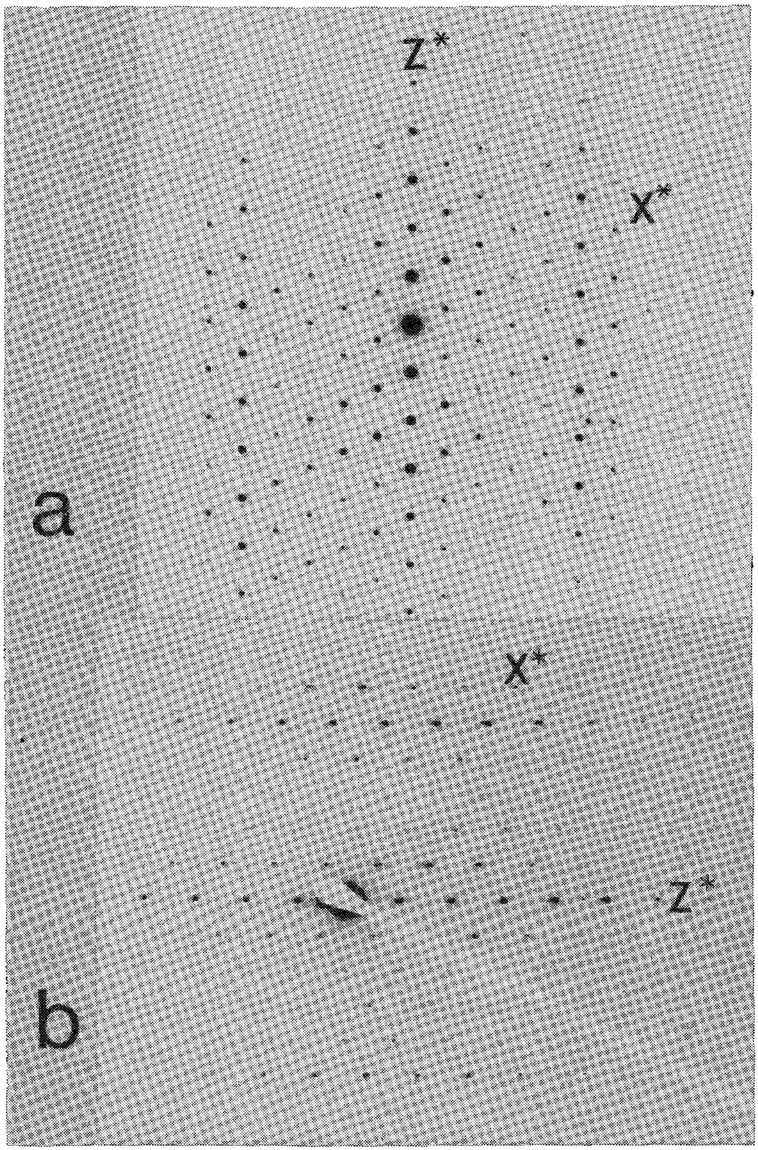

FIG. 3. The $h0l$ net of the P lattice varies considerably from crystal to crystal. The β^* angle has a value of 64° in Figure 3a whereas it has a value of 52° in Figure 3b. However, a feature common to all $h0l$ nets is the sinusoidal variation of intensity along X^*. Both nets are from the minnesotaite sample from Ardua Lake, Quebec. A pseudo a-glide plane ($h0l$, $h = 2n$) is apparent.

Diffraction data: the primitive lattice

In order to emphasize the differences between the orientation of reciprocal lattice planes relative to the electron beam, we define the "true *hk*0 net" as the plane contaning a^*b^*, whereas the "basal plane" is the (001). These two planes are not coincident in minnesotaite. However, describing both planes is beneficial, since the (001) is the cleavage plane and may be oriented rapidly with respect to the electron beam, whereas the a^*b^* plane often is difficult to find.

*The true hk*0 *net and the basal plane.* The *hk*0 net is characterized by strong subcell-reflections (Fig. 2a) along $k = 3n$ layer lines. Parallel to X^*, there are ten superlattice spacings between subcell reflections, indicating that $a = 10 \times 2.8$ Å = 28 Å. Compared to other superlattice reflections, triplets of more intense superlattice reflections occur in a hexagonal pattern symmetrically about each subcell reflection. For example, superlattice reflections with indices 410, 510 and 610 form one of six triplets about the origin, with the 510 reflection being reproduced every 60° rotation about *Z*, but with the 410–510–610 vector maintained parallel to X^*.

Most crystals show streaking parallel to X^* similar to that observed in Figure 2a, although the amount of diffuseness may vary considerably. Also note that *h*00 reflections (*h*0*l* data, $l = 0$) with *h* odd are very weak, indicating a pseudo *a*-glide plane in the structure (see also Fig. 3).

Because minnesotaite is triclinic, X^* is not perpendicular to the cleavage normal (Z^*); hence a diffraction pattern taken with the electron beam normal to a cleavage flake does not represent any crystallographic net in reciprocal space. However, because of the stacking disorder and the consequent Z^* streaking of most reciprocal-lattice nodes, the diffraction pattern of a cleavage flake varies continuously as the flake is tilted out of the (001) plane, rendering zone orientation impossible. Furthermore, because the true *c* axis changes orientation (see below) with almost every layer, a unique orientation parallel to *Z* is impossible to attain. Because of these difficulties, high-resolution images (see below) are presented for the basal plane. In the P cell, the basal plane net differs from the true *hk*0 plane primarily in subtle differences in intensity of subcell reflections (*cf.* Figs. 2a, 2b).

*The h*0*l net.* It is characteristic of all *h*0*l* nets (Fig. 3) that $h = 10n$ rows contain relatively strong maxima in intensity, whereas $h = 10n \pm 2$ rows are weaker and $h = 10n \pm 4$ rows are still weaker. Alternatively, this phenomenon may be described as a sinusoidal variation of intensity along X^*.

The *h*0*l* electron-diffraction pattern differs from crystal to crystal and may vary within parts of a single grain. Although the general appearance of the pattern is similar, unique ß* angles may be measured at approximately 42°, 52° or 64° or, if the sense (+ or –) of the c^* axis is changed, unique angles

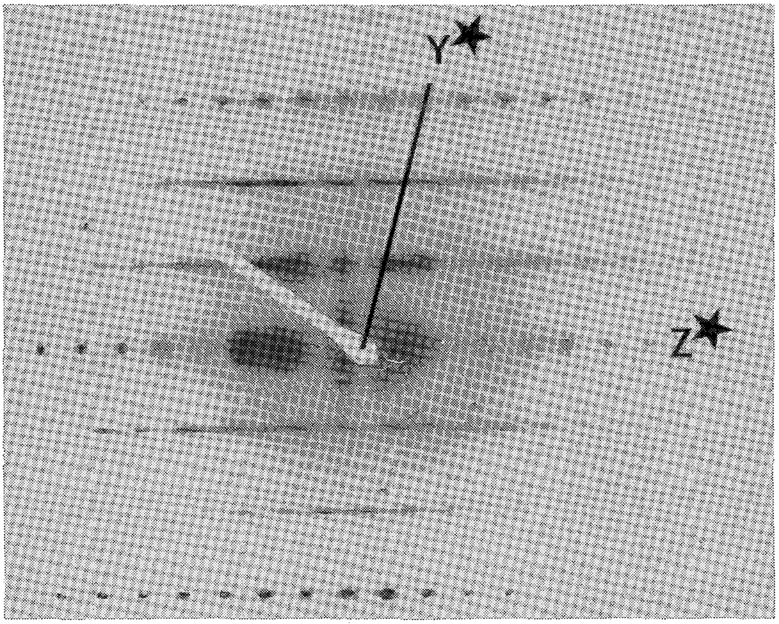

FIG. 4. The 0*kl* net of the *P* structural type has weak *k* odd rows that are most apparent on overexposed photographs. Diffuse streaking parallel to Z^* is characteristic. The sample is from the Auburn mine, Minnesota.

approximately 75°, 46° or 57° may be measured. These β^* measurements are *not* describing a single *h0l* lattice in a different way, but represent observed variations in β^* of different *P* lattices, sometimes within a single grain. Figures 3a and 3b illustrate two variations in β^*. It is remarkable, given the variation in β^*, that crystals may be sufficiently organized to produce sharp maxima at reciprocal-lattice nodes. In particular, 00*l* reflections are usually sharp. However, slight streaking along Z^* (especially for $h = 10n \pm 2$ rows in Fig. 3b) is common and, occasionally, some crystals exhibit a doubling of superlattice reflections and significant streaking along Z^* (and, less commonly, along X^*).

The 0kl net. The 0*kl* net (Fig. 4) is characterized by *very* weak k = odd rows; it is generally necessary to overexpose the 0*kl* net before the k = odd rows become apparent. For all samples examined, these rows show diffuse streaking parallel to Z^*. Although pseudo-0*kl* patterns are superficially similar in spacings and intensities to the true 0*kl* net, the two orientations may be distinguished by the presence, or absence, of these rows.

Reflections with $k = 2n$ also show moderately

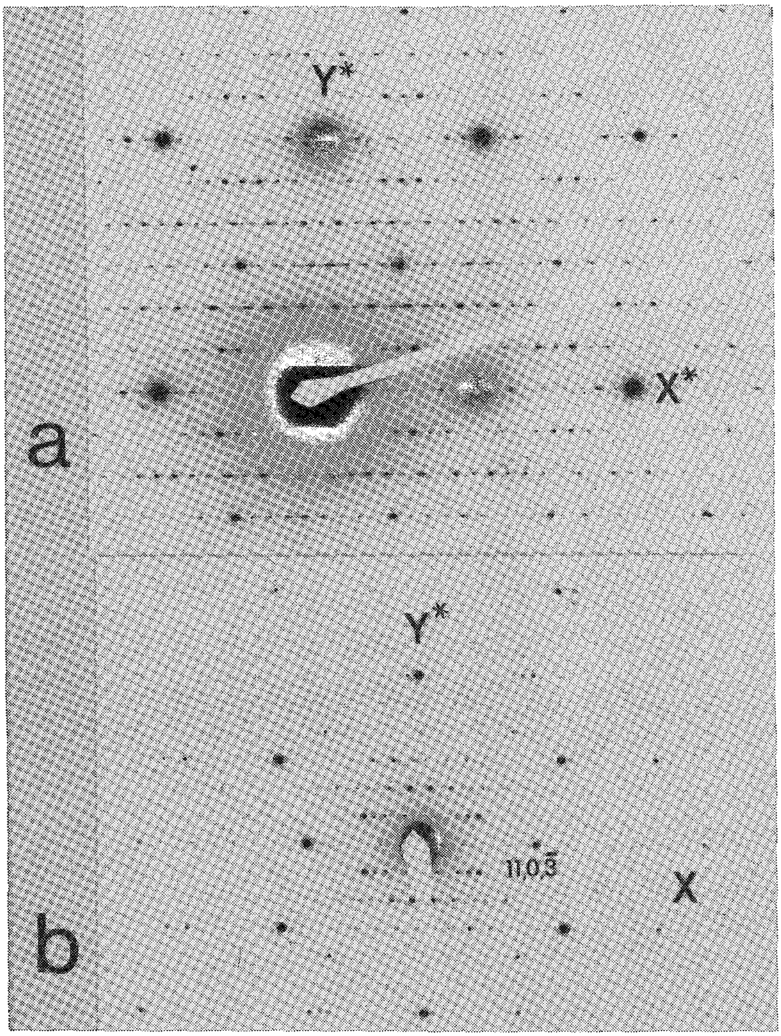

FIG. 5. The *C* lattice *hk*0, net (a, above) is superficially similar to both the *hk*0 net of the *P* cell (*cf.* with Fig. 2a) and the basal-plane net (b). All three nets have strong subcell reflections and superlattice triplets. This net (5a), however, has nine superlattice spacings between strong subcell reflections along X^* as compared to ten for the *P* cell (*cf.* with Fig. 2a) and eleven on the *C*-cell basal plane (5b). All *C*-centred nets are from the Cuyuna district, Minnesota.

diffuse streaking parallel to Z^*, although the $k = 6n$ rows show this effect less than the others. The presence of intensity maxima along these rows allows a choice of α^*, with a measurement of 76.3° ± 0.2° for a one-layer structure. If α^* is chosen to be 90°, then a two-layer modification is described. For the latter, the following conditions for possible reflection may be noted: $k = 4n$ with l = even, and $k = 4n+2$ with l = odd. These conditions suggest that for a unit cell defining a two-layer structure, atoms must repeat at $0,y,z$ and $0,y+¼, z+½$.

Diffraction data: the C-centred lattice

*The true hk*0 *net and the basal plane.* The true $hk0$ net (Fig. 5a) and the basal-plane net (Fig. 5b), although superficially similar, differ in important details. The true $hk0$ has nine superlattice reflections between strong subcell reflections along X^*. This spacing contrasts with eleven observed in the basal plane and the ten found in the true $hk0$ net of the P cell. Because of the C-centring, the ninth observed reflection along X^* is 18,0,0 ($d \sim 2.8$ Å), and a equals 50.6 Å. Other major differences between the true $hk0$ net and the basal-plane net include variations in intensity of subcell reflections similar to those observed for the two nets of the P cell. A rotation about Y^* of approximately 38° is required to relate the two nets.

Similar to the true $hk0$ net of the P cell, the true $hk0$ net of the C cell shows triplets of more intense superlattice reflections about the subcell reflections. In addition, streaking parallel to X^* is common.

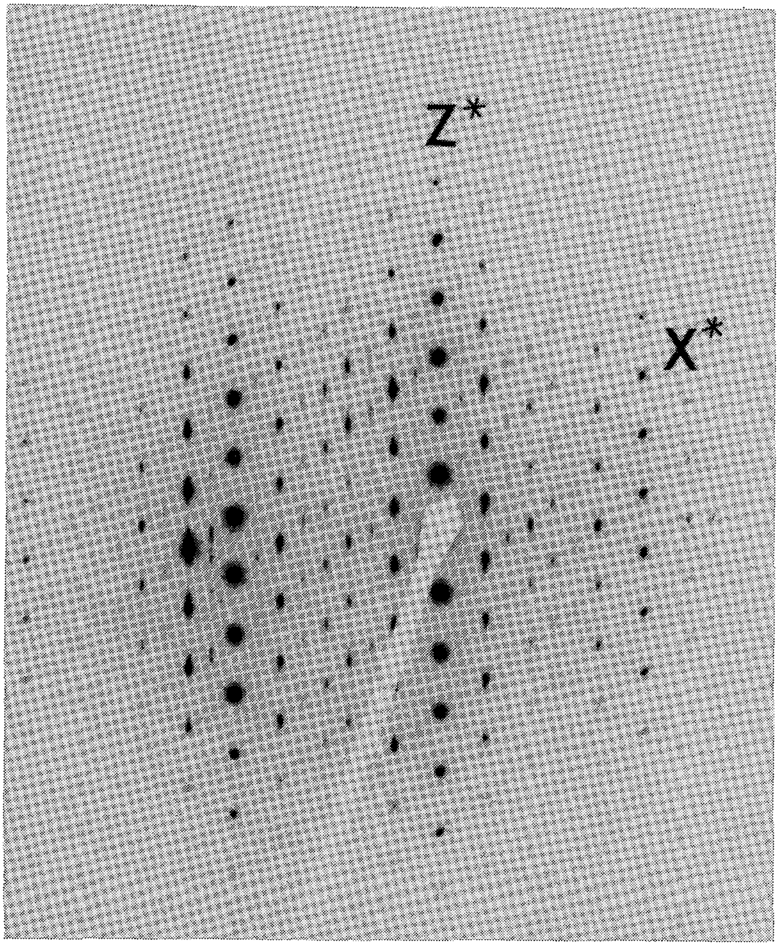

FIG. 6. The $h0l$ net of the C-centred cell has a general sinusoidal distribution of intensities along X^* that reaches a maximum at intervals of $h = 9n$. Note that the unit cell must be approximated because maxima are displaced slightly along Z^* and do not coincide with Bragg positions.

The h0l net (Fig. 6). In contrast to the *P* cell net, the X^* direction of the C-cell net has superlattice spacings with $h = 0, \pm 4, \pm 14$ and ± 18 rows of greater intensity than the other rows. Generally, the rows exhibit a similar sinusoidal variation of intensity as the $h0l$ of the *P* cell, although rows with $h = 18n + 2$ are weak.

The $h0l$ electron-diffraction pattern also has variable β^* angles. In addition, there is sufficient variability within single crystals to produce one-dimension disorder along Z^*. Such disorder is reflected in $h0l$ diffraction patterns by having reciprocal-lattice-node intensity slightly offset from the Bragg position. Diffraction nodes show diffuseness along Z^*, and the unit cell as defined from this net is an average cell.

It is apparent from this net why the superlattice spacings between strong subcell reflections along X^* have a repeat of eighteen in the true $hk0$ net of the *C*-centred cell and an apparent repeat of 22 on the basal plane. The basal-plane net intersects the $h0l$ net at right angles to c^*, thereby passing between reflections on the $h = 18$ layer line but intersecting a strong reflection on the $h = 22$ layer line.

The 0kl net. The $0kl$ net in the *C*-centred lattice differs from what it is in the corresponding *P* lattice in that the weak rows are absent (*cf.* Figs. 7, 4). All other characteristics of the two nets are the same.

THE UNIT CELL AND THE EFFECT OF TWINNING

Because of the variable β^* angle, the unit cell for either the *P* or the *C*-centred lattice is not unique; there are at least three well-crystallized varieties of each and many more poorly organized or average cells. A commonly found cell for both *P* and *C*-centred variants has a β^* of 52°. For purposes of comparison, these cells are given below: *P* cell: $a = 28$ Å, $b = 9.40$ Å, $c = 12.36$ Å, $\alpha \sim 101°$, $\beta \sim 127°$, $\gamma \sim 90°$, space group $P\bar{1}$. *C*-centred cell: $a = 50.6$ Å, $b = 9.42$ Å, $c = 12.36$ Å, $\alpha \sim 101°$, $\beta \sim 127°$, $\gamma \sim 90°$, space group $C\bar{1}$.

The well-crystallized *C*-centred material reported by Guggenheim & Bailey (1982) has a regular periodicity along X^* and corresponds to the *C*-centred cell with β^* of 42°. We have re-examined the single-crystal *X*-ray photographs of Guggenheim & Bailey to reconcile the reported differences in unit-cell parameters.

Intergrowths in minnesotaite can occur either by a translation of structural units by $\pm b/6$ (see discussion below) or by two-fold rotation so that the sense (+ or −) of the *c* axis is reversed. These rotations occur along a twin axis parallel to *X*. The crystal described by Guggenheim & Bailey has both types of twin operations; the former produced an apparent increased superlattice *c*-axis periodicity in the $h0l$

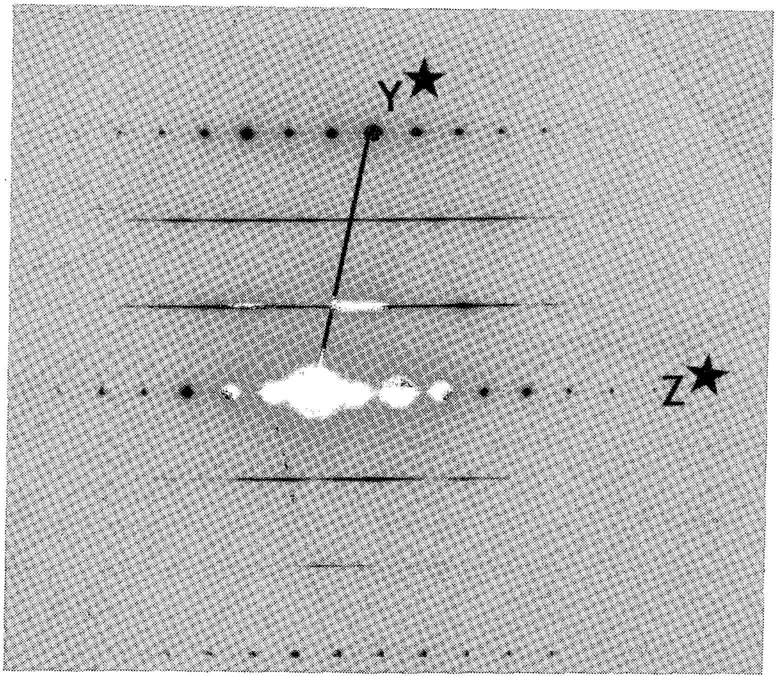

FIG. 7. The *C*-centred cell $0kl$ net shows pronounced streaking along Z^*. The α^* angle may be defined from the maxima on $k \neq 3n$ layer lines.

TABLE 2. X-RAY POWDER DATA, MINNESOTAITE, SAMPLE 1, TABLE 1

hkl	$^1d_{calc}$ (A)	$^2d_{obs}$ (A)	$^3I/I_o$	*hkl*	d_{calc} (A)	d_{obs} (A)	I/I_o
001	9.54	9.54	100(100)	$33\bar{4}$	1.597	1.597	6B(15)
002	4.77	4.78	15(20)	$33\bar{7}$	1.596		
		4.62	5B(10)	$\bar{3}36$	1.575	1.576	8
003	3.18	3.18	50(50)	$06\bar{1}$	1.565	1.565	13(20)
$\bar{2}04$	2.798	2.796	2	$06\bar{2}$	1.564		
$20\bar{3}$	2.759	2.759	25(22)	$1\bar{3}4$	1.548	1.541	2(10)
$13\bar{3}$	2.721	2.721	15	$3\bar{3}\bar{3}$	1.543		
$\bar{1}32$	2.652	2.655	35(22)	$\bar{3}\bar{3}8$	1.543		
$\bar{1}\bar{3}4$	2.537	2.538	25 (70)	060	1.525	1.524	2(5)
$20\bar{2}$	2.525	2.528	45	$0\bar{6}3$	1.523		
$\bar{1}\bar{3}3$	2.403	2.405	32(20)	$\bar{2}09$	1.509	1.509	5B(10)
$1\bar{3}1$	2.351	2.356	5	$33\bar{4}$	1.506		
$\bar{2}06$	2.316	2.318	12(5)	$\bar{3}37$	1.505		
$\bar{1}\bar{3}5$	2.250	2.248	15(5)	133	1.452	1.450	2(10)
$20\bar{1}$	2.212	2.212	20(20)	$0\bar{6}4$	1.451		
$1\bar{3}4$	2.103	2.103	10(10)	$\bar{4}09$	1.365	1.362	8B(15)
$1\bar{3}2$	2.051	2.050	5	007	1.363		
$\bar{2}07$	2.005	2.007	10(5)	062	1.362		
$\bar{1}\bar{3}6$	1.954	1.956	5(5)	$26\bar{4}$	1.352	1.351	8B(15)
131	1.912	1.913	10(10)	$2\bar{6}\bar{1}$	1.352		
200	1.911			$\bar{2}$,0,10	1.328	1.325	8B(15)
$\bar{1}35$	1.822	1.822	4(10)	$\bar{2}64$	1.326		
$\bar{1}\bar{3}7$	1.695	1.695	5(5)	$\bar{2}\bar{6}7$	1.325		
201	1.655	1.656	5(10)	$\bar{3}39$	1.308	1.307	5B(10)
$33\bar{6}$	1.608	1.609	15(20)	$2\bar{6}0$	1.308		
$\bar{3}35$	1.608			$\bar{4}$,0,10	1.308		
				$\bar{1}\bar{3}9$	1.306		

1. calculated *d*-values based on a=5.623(2)Å, b=9.419(2)Å, c=14.234(5)Å, α=99.44(3)°, β=136.35(2)° and γ=90.00(2)°.

2. *d*-values obtained with 114.6 mm Gandolfi camera using monochromatic FeKα radiation (=1.9373A); see Guggenheim & Bailey (1982).

3. Intensity data visually estimated from the Gandolfi photograph. Figures in parentheses are visually estimated from a Debye-Scherrer photograph using non-monochromatic FeKα radiation as given in Blake (1965).

net that was not recognized as related to twinning in the earlier study. Note that these reflections are connected by diffuse streaking, indicating a coherency of intergrowth. The apparent increase in periodicity of the superlattice *a*- and *b*-axes resulted from higher-level superlattice reflections passing through the layer-line screen. In summary, both sets of data are consistent with the unit cell reported here. The reciprocal-cell data of the *C*-centred lattice given by Guggenheim & Bailey (1982) may be transformed to a subcell whose reciprocal axes are parallel to those of the superlattice by the matrix

$$\begin{aligned} a_{GE} &= -1a_{GB} + 0b_{GB} + 2c_{GB} \\ b_{GE} &= 0a_{GB} + 1b_{GB} - \tfrac{1}{3}c_{GB} \\ c_{GE} &= 0a_{GB} + 0b_{GB} + 1c_{GB} \end{aligned}$$

Table 2 gives the indexed powder-pattern for the *C*-centred lattice referred to these axes. The *d*-value at 4.62 Å is attributed to superlattice reflections and has not been indexed here (see Guggenheim & Bailey 1982).

HIGH-RESOLUTION IMAGING, INTERPRETATION AND MODEL OF THE STRUCTURE

Bright-field images were formed by the introduction through the objective aperture of all reflections within a radius of 0.5 Å^{-1} for both the basal plane (Fig. 8) and the *h*0*l* nets (Fig. 9). The structural images of Figures 8 and 9 provide a straightforward description of the minnesotaite structure, within the constraints of resolution. Figure 9 shows an uninterrupted row of dots with maxima every 3.3 Å, which is interpreted as a continuous octahedral sheet with iron atoms possibly resolved. On either side of the octahedral sheet are discontinuous bands that are consistent with short lengths of connected tetrahedra. The shorter bands are 9 Å and are equivalent in width to three linked tetrahedra, whereas the longer are 12 Å, which is equal to four linked tetrahedra. Figure 8 illustrates that these tetrahedral linkages extend along *Y* infinitely, as is consistent with the short *b*-axis periodicity of 9.42 Å. Therefore, the structure may be described as consisting of strips of tetrahedra either three or four tetrahedra wide on either side of a sheet of octahedra. In the interlayer region, there is electron density between tetrahedral strips (Fig. 9). To be consistent with a talc-like chemistry and the X-ray-diffraction data, this electron density must be interpreted as two tetrahedra that serve to connect adjacent layers. In some especially well-resolved areas of the image, the electron density appears to be split, with each part possibly representing a tetrahedron in projection. The measured width of these regions is 6 Å, consistent with this interpretation. Where the tetrahedral apices are inverted, an OH group is required to complete octahedral coordination about the iron ions. This is in accord with the chemical determinations that indicate an excess in hydroxyl relative to the normal structure of talc.

The tetrahedral strips are offset across the octahedral sheet (Fig. 9c) so that there are only small regions of 2:1 layer character. This arrangement allows the octahedral sheet to warp or to become wave-like, although the details of this are apparent only in some areas of Figures 9a and b. In addition, particularly near the junction where the tetrahedral strips and inverted interlayer tetrahedra join, the tetrahedra in the strips tilt out of plane to cause a slight warping effect. The diffraction evidence for these effects is discussed in more detail below.

It is evident that there is considerable irregularity associated with the placement of the strips of tetrahedra on either side of the octahedral sheet. Although the image from the *h0l* net of the *P* cell (Fig. 9a) is dominated by strip-width sequences involving four tetrahedra, width sequences involving the alternation of three and four tetrahedra may be found, as well as random sequences. These sequences have a significant effect on β^* values and correlate with the variations observed in *h0l* diffraction patterns (see above). Note also that the irregularity in width of the tetrahedral strip along *X* makes further interpretation of the structural image of the basal plane (Fig. 8) difficult, because this image requires a projection down c^*. Figure 9b, the image from the *h0l* net of the *C*-centred cell, differs primarily from Figure 9a in that strip-width sequences involving the alternation of three and four tetrahedra dominate the structure. It is noteworthy that in some images (not shown) there are occasionally tetrahedral strip-width sequences that include five tetrahedra, and several areas have been located that have *d*(001) = 7 Å and that are antigorite-like in character.

DISCUSSION AND FURTHER INTERPRETATION

The X-ray structure analysis indicates that minnesotaite has a talc-like 2:1 layer, but that approximately one quarter of the silicon atoms are missing from the continuous tetrahedral sheet and that the

FIG. 8. The bright-field image of the basal plane of the *C*-centred cell net (Cuyuna district sample) shows that the structural features of minnesotaite are continuous along *Y*, but perturbations occur along *X*.

missing atoms are to be found between the 2:1 layers. The high-resolution images confirm this analysis, but neither technique can provide the necessary resolution accurately to describe details. For example, the relative positions and spacings of adjacent strips of tetrahedra would partially establish connectivity of tetrahedra between adjacent layers, but this information cannot be derived from the images or X-ray-subcell data. The *hk*0 diffraction net contains this information, but diffraction patterns of large superstructures are difficult to compute, even if the structure is known generally. From a practical viewpoint, input data are unwieldy, and computer times are long for a structure with a large number of parameters. Further problems arise in computing patterns from disordered structures, such as that of minnesotaite, and the output, whether numerical or half-tone, is difficult to assess. In addition, to solve a superstructure by trial-and-error procedures through numerical calculations would be laborious. By contrast, an optical diffraction pattern (Taylor & Lipson 1964), produced from a two-dimensional mask representing a projection of the structure, is easy and inexpensive to produce and may be rapidly compared to an electron- or X-ray-diffraction pattern.

Layer silicates are composed of two major substructures, the octahedral and the tetrahedral sheets. The octahedral sheet, which is usually comprised of heavy atoms, dominates the diffraction pattern and impresses a hexagonal distribution of intensity on the Fourier transform. For example, in the *hk*0 net of talc, micas, *etc.*, maxima occur in the *C*-centred cell at positions of indices 200, 130 and $1\bar{3}0$ and 060, 330, $3\bar{3}0$, with each group being pseudosymmetrically equivalent (hexagonal). If the tetrahedral sheet is commensurate with the octahedral sheet, the Fourier transform from the tetrahedral portion will have maxima at the same *hk* indices, as well as subsidiary maxima at 110, 020, $1\bar{1}0$, *etc.*, produced by the larger size of the tetrahedral repeat unit. For the purposes of model development, we may initially consider the sheets of tetrahedra and octahedra as 'semi-independent', so that their lateral dimensions do not have to be congruent. For cases in which the

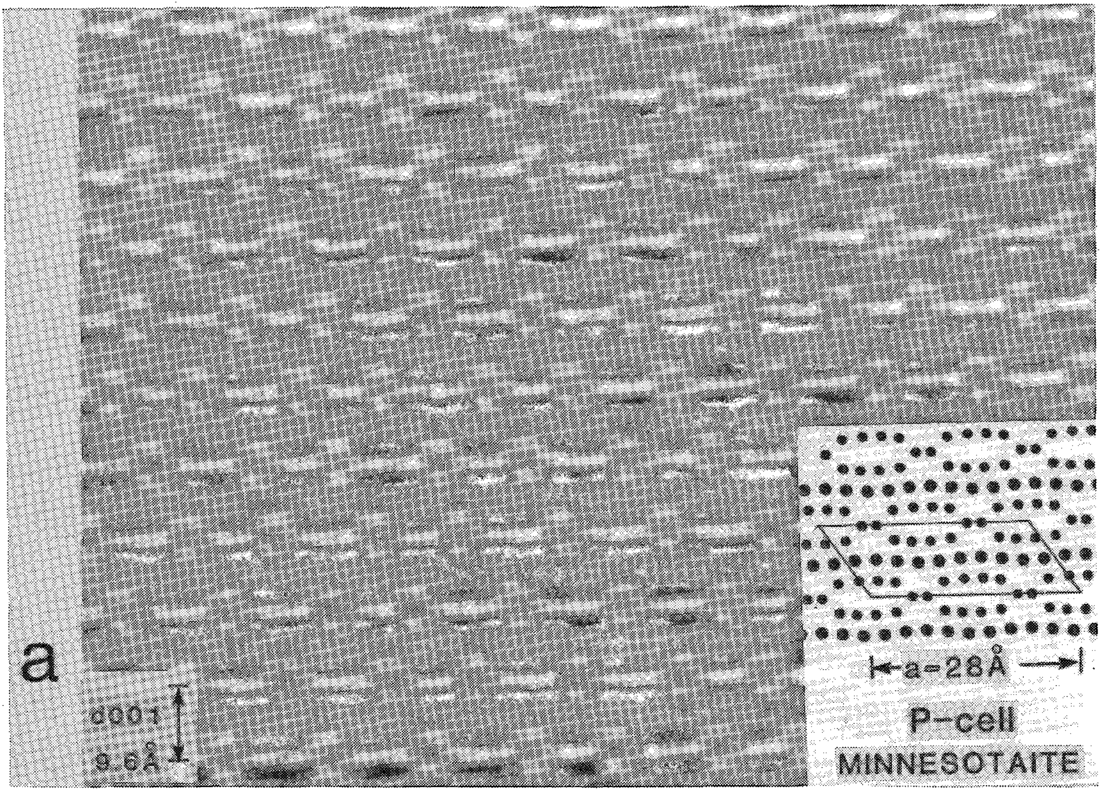

FIG. 9a. The bright-field high-resolution image of the *h*0*l* net of the *P* cell (Ardua Lake sample) showing the continuous nature of the Fe octahedral sheet and the modulated tetrahedral sheets. Intensity distribution between the layers is interpreted as inverted tetrahedra that serve to connect the layers. Several examples of β are given. See the appropriate sections for further discussion.

tetrahedral sheet is not of the same size as the octahedral sheet, the Fourier transform of the tetrahedral sheet will reach maxima at positions displaced from those due to the Fourier transform of the octahedral sheet. Normal layer silicates do not show such displacements because the tetrahedral and octahedral sheets are commensurate and, also, because the Bragg reflections are widely spaced. However, in

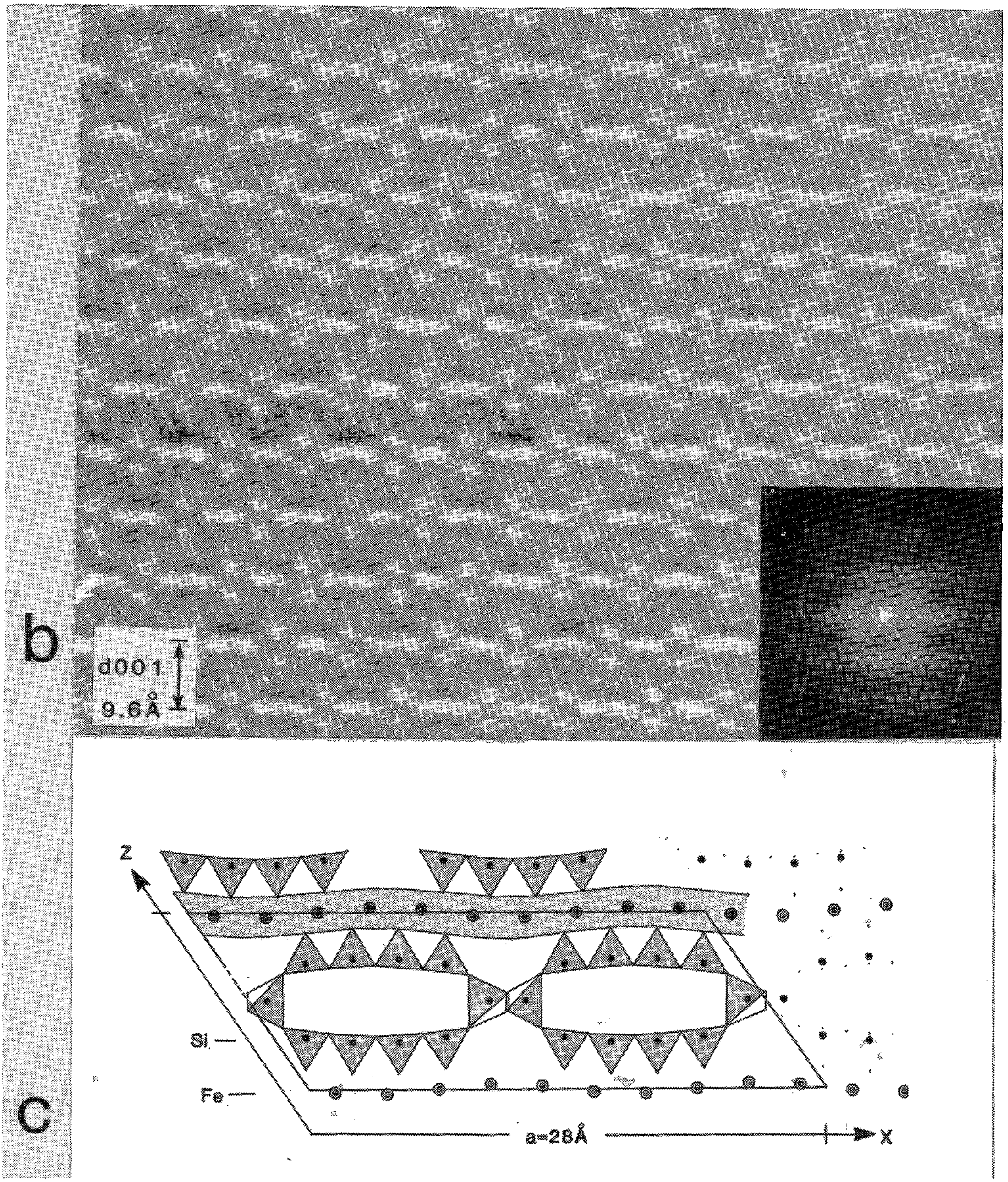

FIG. 9b. This *h*0*l* image, for the *C*-centred cell (Cuyuna district sample), differs primarily from that in Figure 9a in that the strip widths alternate with sequences involving 3 and 4 tetrahedra, whereas Figure 9a is dominated by strip-width sequences of 4 tetrahedra. (c) Diagram of the *P*-cell structure viewed down *Y*. (The interlayer tetrahedra are actually corner-shared.)

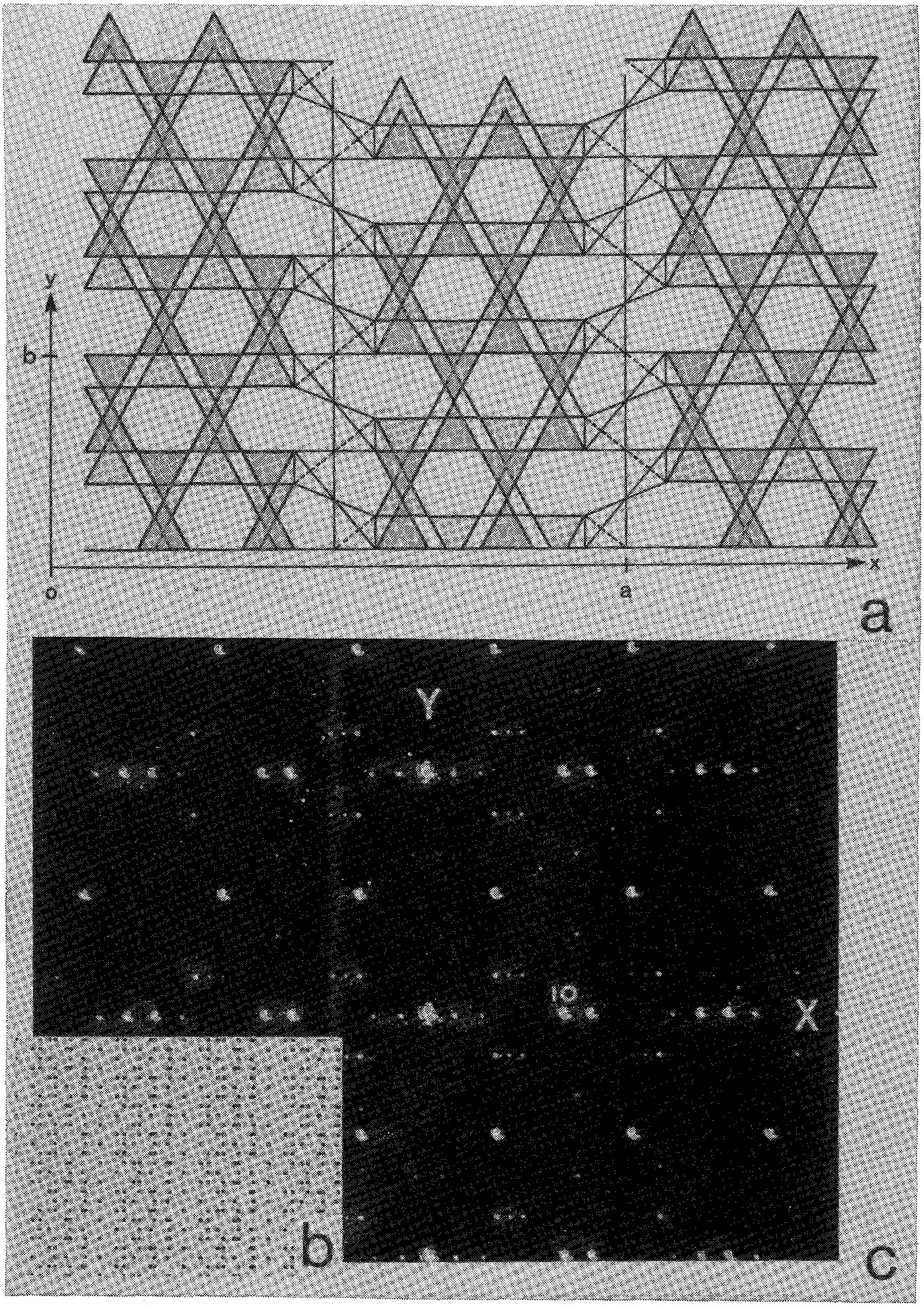

FIG. 10. Aspects of the minnesotaite structures and optical diffraction patterns from models: (a) *P* cell, showing adjacent 4-tetrahedra-wide strips connected across the interlayer region by chains of tetrahedra. (b) Optical diffraction mask, including Fe, Si and O. (c) Optical diffraction pattern (compare Fig. 2b).

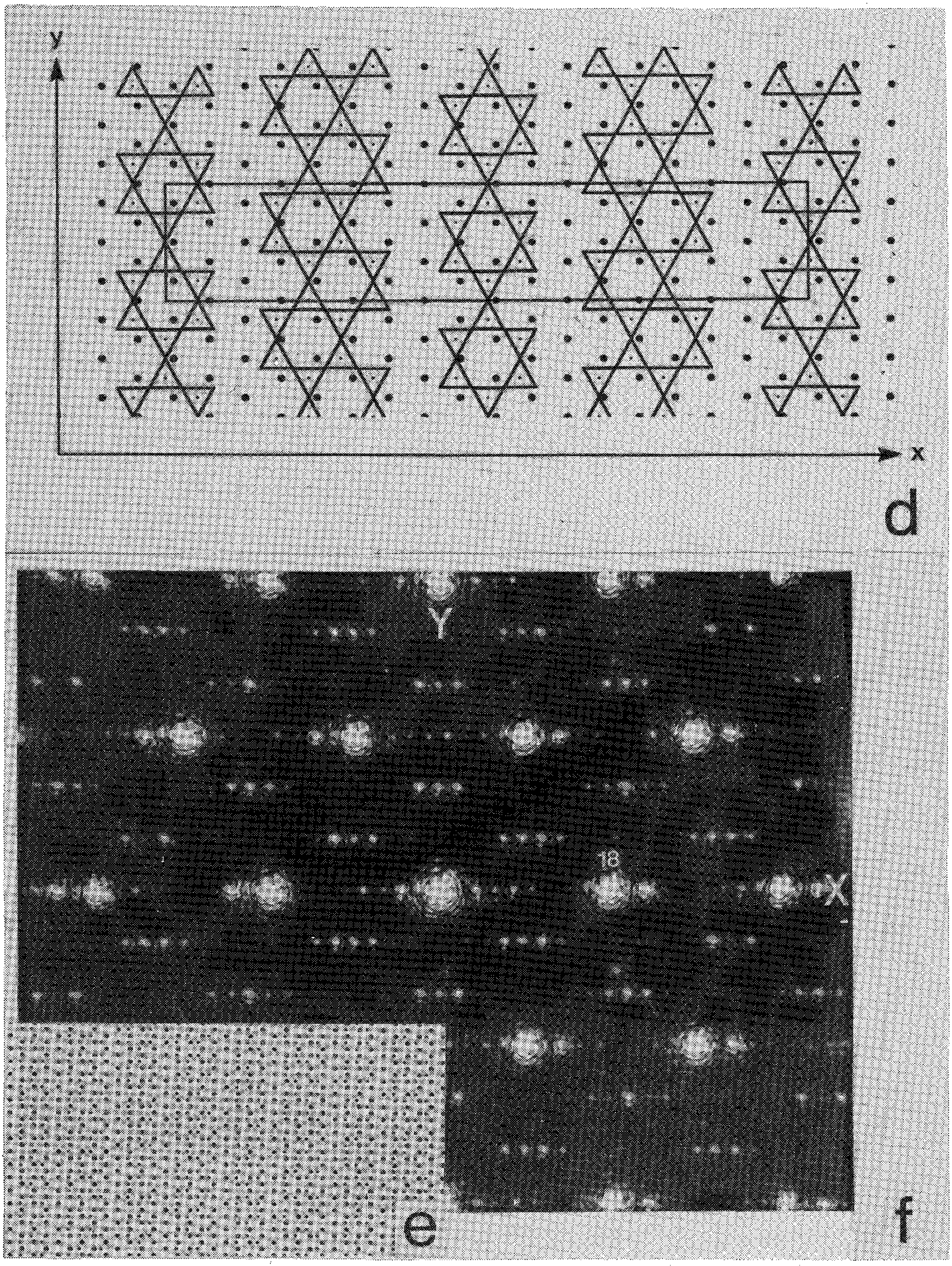

FIG. 10. (cont'd). Aspects of the minnesotaite structures and optical diffraction patterns from models: (d) *C* cell, showing octahedrally co-ordinated cations and one level of tetrahedral strips, alternately 3- and 4-tetrahedra wide. (e) Diffraction mask. (f) Optical diffraction pattern (*cf.* Fig. 5b).

structures with superlattices caused by a small structural perturbation, the Fourier transform approaches a continuum, which allows detail in the transform to be interpreted. It is on the basis of this detail and the observed displacements of maxima that we have modeled the *hk*0 diffraction data for minnesotaite; the displacements are caused by lateral misfit between a larger sheet of $Fe(O,OH)_6$ octahedra and a smaller sheet of SiO_4 tetrahedra.

The intensity distribution for observed reflections along *a**, the superlattice direction in minnesotaite, is an important aspect of the interpretation of the structure. Reflection 800 is weak, 10,0,0 is very strong and 12,0,0 is medium. The 10,0,0 in minnesotaite ($d_{10,0,0} = 2.8$ Å) corresponds to the d_{200} for an analogous layer silicate without a superlattice, such as talc. This intensity distribution suggests that the Fourier transform of the component sheets reaches a maximum at $10 < h < 12$ rather than exactly at $h = 10$. This results from the tetrahedral sheet being smaller than the octahedral sheet.

An intriguing feature of the *hk*0 net is the distribution of triplets of more intense superlattice-reflections symmetrically located about each subcell reflection. Optical modeling shows that these reflections are produced when two strips of tetrahedra parallel to *Y*, each four tetrahedra wide, are equally spaced over ten octahedra.

Additional optical simulations for a structure with a wave-like octahedral sheet produce a sinusoidal distribution of intensity such as that observed on the *h*0*l* net. Some flexing of the octahedral sheet would be anticipated when strips of tilted tetrahedra are offset across the octahedral sheet. Note that the wave-like nature of the octahedral sheet is observed only in selected positions of Figure 9, but the diffraction evidence suggests that it is a common feature of the structure. The X-ray *h*0*l* direct Fourier map of the subcell is also in agreement with this interpretation, since it was possible to model the iron ions on the basis of half atoms with displacements along *Z**.

The *C*-cell material has a composition $Fe_{27}Si_{36}O_{86}(OH)_{26}$, and the *P*-cell, $Fe_{30}Si_{40}O_{96}(OH)_{28}$. Mg substitutes for Fe more extensively in the *P*-cell structure. There is little substitution of Si by Al. The ideal chemical formulae of the subcells are: *C* cell: $Fe_3Si_4O_{9.55}(OH)_{2.89}$, *P* cell: $Fe_3Si_4O_{9.6}(OH)_{2.8}$. They contain significantly more (OH) than normal talc, but are consistent with the structural formulae calculated to +22 (Table 1).

Finer details of the *hk*0 diffraction net of minnesotaite can be modeled by varying the displacements of adjacent tetrahedral strips parallel to *Y*. The model presented here (Figs. 10a, c) gives a satisfactory match in intensity between the electron and optical diffraction patterns, when adjacent tetrahedral strips *a*/2 apart are displaced by *b*/2 on one side of the interlayer and *b*/6 on the other. Such displacements give atomic co-ordinates (relative to 001 normal) of (x, y, z), $(x + ½, -y, z)$ and so give rise to a pseudo *a*-glide plane in the *P* cell. In the *C*-centred cell, *h*00 reflections with *h* odd absent is a condition required by the lattice type. Streaking parallel to *X**, commonly observed, occurs when adjacent tetrahedral strips are displaced semirandomly.

Attempts to use optical simulation methods to model the spatial relationship of the strips of tetrahedra between adjacent layers fail, because the observed *hk*0 diffraction pattern (Figs. 2a, 5a) is essentially the Fourier transform of an individual layer. Disorder parallel to (001) introduces diffuseness along *Z**, as is apparent in the 0*kl* diffraction pattern (Figs. 4, 7). Therefore, there is no single translation-vector *c* between one layer and another. It is only possible to represent the octahedral sheet and its adjacent tetrahedral sheet because these have the same relationship in all layers. It is possible, however, to place constraints on the disposition of the tetrahedral strips between adjacent layers by using arguments based on crystal chemistry.

In order to be consistent with $b = 9.4$ Å, $d(001) \sim 9.6$ Å, tetrahedra in the interlayer region must link adjacent tetrahedral strips by a chain parallel to *Y*, having tetrahedral edges approximately parallel to *Y* and to *Z** (Fig. 10a). Therefore, the interlayer separation is similar to that observed in talc or pyrophyllite (~2.7 Å). In these structures, because the three basal anions in a tetrahedron are not efficient electrostatic shields for opposing Si ions, the 6-member rings of SiO_4 tetrahedra are offset across the interlayer so that rings of tetrahedra are not directly superimposed. Such an arrangement reduces the repulsive effects that would occur if poorly shielded silicon ions directly opposed each other across this narrow interlayer region. Our model considers that similar forces would be acting in minnesotaite; the model features silicon ions projecting over the edges of tetrahedra in adjacent layers, as in talc. The structural arrangement presented here is consistent with the observed α^* and β^* angles. Because the rings of tetrahedra across the interlayer do not superimpose, there is no cation site available for larger cations, such as K, Na and Ca. Small amounts of alkali present in the chemical composition (Table 1) may be accomodated in positions that occasionally occur through positional errors (associated with tetrahedral strip and layer placement) or as a result of impurity phases.

Finally, note that the misfit between tetrahedral and octahedral sheets, although responsible for the development of a superlattice along *X*, is accommodated along *Y* without a major structural modification. Perturbations along *X* are common in the Mg-rich serpentine antigorite, but the Fe-rich serpentine, greenalite, is island-like, with structural modifications to relieve strain along *Y* as well. In minnesotaite, tetrahedral strip widths are narrow (3 and 4 tetrahedra wide) compared to the seven tetrahedra found across the island in greenalite. Strip widths of this size may allow sufficient octahedral distortions along *Y* to relieve strain, particularly near strip edges. Note that the most iron- and silicon-rich minnesotaite (Table 1, no. 1), which has the largest misfit between the tetrahedral and octahedral sheets, requires more perturbations for a given distance along *X* than other compositions, because the *C*-centred cell has an average strip-width of 3½ tetrahedra. On the other hand, the two structural modifications often occur together; the Cuyuna minnesotaite has a relatively small amount of *P*-cell character, and the most Mg-rich minnesotaite from the Sokoman Iron Formation (Table 1, no. 7) has some *C*-lattice intergrowths. These observations suggest that composition can vary slightly even within a single grain.

ACKNOWLEDGEMENTS

This study was supported by the Experimental and Theoretical Geochemistry Program and the U.S.-Australia Co-operative Science Program of the U.S. National Science Foundation under grant EAR80-18222. We thank Professor B.G. Hyde for use of the electron-microscope facilities and G. Robertson for advice and use of the X-ray-crystallography programs; both of them are at the Research School of Chemistry, Australian National University. Specimens were kindly provided by R.L. Blake, G.A. Gross, C. Klein, C.M. Lesher and J.J. Papike. We thank Dr. J.D.H. Donnay of McGill University for carefully reviewing the manuscript.

REFERENCES

BAILEY, S.W. (1980): Structures of layer silicates. *In* Crystal Structures of Clay Minerals and their X-ray Identification (G.W. Brindley & G. Brown, eds.). Mineralogical Society, London.

BLAKE, R.L. (1965): Iron phyllosilicates of the Cuyuna district in Minnesota. *Amer. Mineral.* **50**, 148-169.

EGGLETON, R.A. (1972): The crystal structure of stilpnomelane. II. The full cell. *Mineral. Mag.* **38**, 693-711.

______ & BAILEY, S.W. (1967): Structural aspects of dioctahedal chlorite. *Amer. Mineral.* **52**, 673-689.

______ & GUGGENHEIM, S. (1986): The superlattice of ganophyllite. *Mineral. Mag.* (in press).

GRUNER, J.W. (1944): The composition and structure of minnesotaite, a common iron silicate in iron formations. *Amer. Mineral.* **29**, 363-372.

GUGGENHEIM, S. & BAILEY, S.W. (1982): The superlattice of minnesotaite. *Can. Mineral.* **20**, 579-584.

______, ______, EGGLETON, R.A. & WILKES, P. (1982): Structural aspects of greenalite and related minerals. *Can. Mineral.* **20**, 1-18.

JAGODZINSKI, H. & KUNZE, G. (1954): Die Röllchenstruktur des Chrysotils. I. Allgemeine Beugungstheorie und Kleinwinkelstreuung. *Neues Jahrb. Mineral. Monatsh.*, 95-108.

KUNZE, G. (1956): Die gewellte Struktur des Antigorits. *I. Z. Krist.* **108**, 82-107.

LEITH, C.K. (1903): The Mesabi iron-bearing district of Minnesota. *U.S. Geol. Surv. Mon.* **43**.

LESHER, C.M. (1978): Mineralogy and petrology of the Sokoman Iron Formation near Ardua Lake, Quebec. *Can. J. Earth Sci.* **15**, 480-500.

LOPES-VIEIRA, A. & ZUSSMAN, J. (1969): Further detail on the crystal structure of zussmanite. *Mineral. Mag.* **37**, 49-60.

NORTH, A.C.T., PHILLIPS, D.C. & MATHEWS, F. (1968): A semi-empirical method of absorption correction. *Acta Cryst.* **A24**, 351-359.

PERRAULT, G. & HÉBERT, P. (1968): Minnesotaite from the Bluebell mine, Riondel, B.C. *Can. Mineral.* **9**, 579 (abstr.).

RADOSLOVICH, E.W. (1961): Surface symmetry and cell dimensions of layer lattice silicates. *Nature* **191**, 67-68.

TAYLOR, C.A. & LIPSON, H. (1964): *Optical Transforms, their Preparation and Application to X-ray Diffraction Problems.* G. Bell and Sons, London.

ZUSSMAN, J. (1954): Investigation of the crystal structure of antigorite. *Mineral. Mag.* **30**, 498-512.

ZVIAGIN, B.B. (1957): Determination of the structure of celadonite by electron diffraction. *Sov. Phys. Cryst.* **2**, 388-394.

Received September 30, 1985, revised manuscript accepted February 15, 1986.